Geophysical Research Letters

RESEARCH LETTER
10.1029/2018GL077737

Key Points:
- A balloon-borne infrasound microphone flew over an ocean microbarom source
- Maximum upgoing acoustic energy flux was 0.05 mW/m^2
- Dissipating ocean microbarom acoustic waves may heat the thermosphere by several Kelvins per day

Supporting Information:
- Supporting Information S1
- Audio S1

Correspondence to:
D. C. Bowman,
dbowma@sandia.gov

Citation:
Bowman, D. C., & Lees, J. M. (2018). Upper atmosphere heating from ocean-generated acoustic wave energy. *Geophysical Research Letters*, *45*, 5144–5150. https://doi.org/10.1029/2018GL077737

Received 3 NOV 2017
Accepted 9 APR 2018
Accepted article online 27 APR 2018
Published online 21 MAY 2018

Upper Atmosphere Heating From Ocean-Generated Acoustic Wave Energy

D. C. Bowman[1] and **J. M. Lees**[2]

[1]Sandia National Laboratories, Albuquerque, NM, USA, [2]Department of Geological Sciences, University of North Carolina at Chapel Hill, Chapel Hill, NC, USA

Abstract Colliding sea surface waves generate the ocean microbarom, an acoustic signal that may transmit significant energy to the upper atmosphere. Previous estimates of acoustic energy flux from the ocean microbarom and mountain-wind interactions are on the order of 0.01 to 1 mW/m^2, heating the thermosphere by tens of Kelvins per day. We captured upgoing ocean microbarom waves with a balloon-borne infrasound microphone; the maximum acoustic energy flux was approximately 0.05 mW/m^2. This is about half the average value reported in previous ground-based microbarom observations spanning 8 years. The acoustic flux from the microbarom episode described here may have heated the thermosphere by several Kelvins per day while the source persisted. We suggest that ocean wave models could be used to parameterize acoustically generated heating of the upper atmosphere based on sea state.

Plain Language Summary When two sets of ocean waves collide, they generate the sea surface equivalent of a gigantic subwoofer. The resulting low-frequency sound waves can travel across the planet and even heat the upper atmosphere. While this heating has been estimated using distant ground-based measurements, no one has actually measured the strength of the sound waves directly above the source. Using a microphone on a high-altitude balloon, we intercepted these upgoing waves and directly measured their energy content for the first time. We found that they carry an energy flux of about 0.05 mW/m^2. For context, one would have to capture all the acoustic energy over a 1.2-km^2 region to illuminate a single 60-W lightbulb. Even so, the energy is sufficient to heat the upper atmosphere by several degrees Celsius per day. This is consistent with previous modeling studies.

1. Introduction

A variety of Earth surface and atmospheric phenomena generate acoustic waves. These waves are usually in the subaudible or "infrasound" (<20 Hz) range. The upgoing portion of this geoacoustic wavefield is strongly attenuated in the mesosphere and thermosphere, resulting in a net energy transfer from the lower to the upper atmosphere. This may raise the temperature of the mesosphere/lower thermosphere region by up to several tens of Kelvins per day (Maeda, 1964; Rind, 1977). Sources of this acoustic energy flux include ocean waves (Rind, 1977), thunderstorms (Davies & Jones, 1973; Hickey et al., 2001; Walterscheid et al., 2003), wind interacting with mountains (Semenov et al., 2012), and explosions (Drobzheva & Krasnov, 2006). Energy flux estimates derived from ground-based infrasound measurements (Rind, 1977) and upper atmosphere observations (Davies & Jones, 1973; Semenov et al., 2012) range from 0.04 to 3 mW/m^2. This is comparable to energy contributions via atmospheric tides (Hines, 1965) and 1 to 2 orders of magnitude less than that of gravity waves (Gossard, 1962).

No study to date has directly intercepted the upgoing acoustic wavefield between its source and dissipation region, and thus, energy flux estimates rely on ground-based measurements (Rind, 1977) or airglow observations (Semenov et al., 2012). Since the structure of the troposphere typically refracts sound waves upward, a receiver on the Earth's surface usually records direct acoustic arrivals from a ground-based source at ranges of only a few tens of kilometers. At greater distances, ground sensors detect waves refracted back downward toward the Earth as a result of temperature and wind variations or the extreme temperature gradients in the upper atmosphere (Figure 1). Certain atmospheric configurations, such as strong tropospheric winds, the biannual stratospheric wind minimum, and mesospheric winds, can cause acoustic propagation patterns to deviate from those described above. Waves refracted from the stratosphere and thermosphere back to Earth

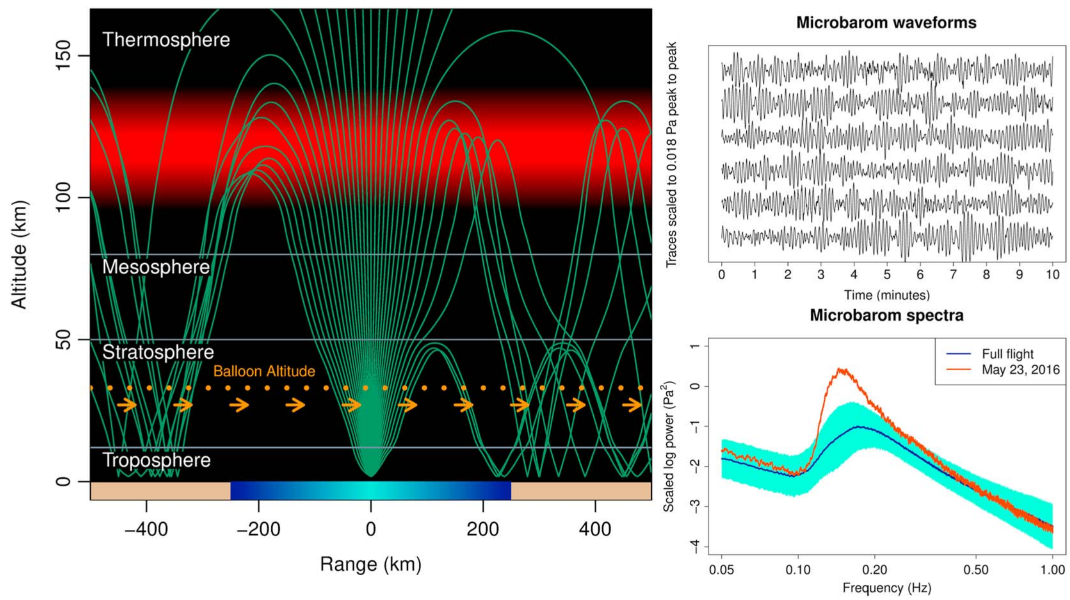

Figure 1. (Left) Typical stratospheric and thermospheric ocean microbarom propagation paths. Microbaroms are generated in the open ocean and can be detected on land via refractions from temperature gradients in the thermosphere and winds in the stratosphere. Direct arrivals can be recorded on free flying platforms only. The red shaded region of the thermosphere indicates where the microbarom dissipates, depositing its energy as heat. (Right) A 1-hr recording of ocean microbarom waveforms (top) and a daylong Welch spectrum (bottom) during the balloon's overflight of the source region compared with the average Welch spectrum of the full observation period. The light blue band is the standard deviation of the flight spectrum.

have been modified via intrinsic and geometric attenuation due to their long propagation paths as well as nonlinear effects at ray caustics (Rogers & Gardner, 1980) and an exponential decrease in air density (Lonzaga et al., 2015). They may not be an accurate representation of the solely upgoing infrasound flux. Airglow observations can capture temperature variations in the middle and upper atmosphere (Semenov et al., 2012) but lack the temporal resolution required to image short-period waves such as infrasound. The most direct way to isolate and characterize acoustic energy flux is to capture the infrasound signals as they propagate from the lower to the upper atmosphere; this is the focus of our study.

One of the most pervasive infrasound signals is the ocean microbarom (Bowman et al., 2005). The waves have a frequency of 0.13–0.35 Hz with a characteristic amplitude-modulated signature (Campus & Christie, 2010) (see Figure 1). Hereafter we refer to this as the *microbarom band*. The signal arises from nonlinear interactions of opposing surface wave trains in the open ocean (Waxler & Gilbert, 2006). Because of the source region's distance from land, direct microbarom arrivals have likely never been measured, and their energy input to the upper atmosphere has not been directly quantified. However, observations of thermospherically refracted microbaroms at sensors located in Palisades, New York, led to upper atmosphere energy inputs estimated to be about 0.1 mW/m^2, for a daily heating rate of up to 30 K between 105- and 140-km altitude (Rind, 1977).

Recent experiments have shown that microphones on high-altitude balloons often record the ocean microbarom (Bowman & Lees, 2017). We report results from one such flight, in which the microphones flew directly over an actively radiating ocean microbarom source region southeast of New Zealand. The upgoing acoustic wave energy in the ocean microbarom band during the source overflight was about 0.05 mW/m^2. The ocean microbarom was nearly continuous during the flight (see Figure 2), in contrast to ground stations where it is sometimes obscured by wind noise, particularly during the day (Bowman et al., 2005). The ocean microbarom frequency and amplitude variations visible in Figure 2 are especially apparent when the infrasound data are sped up into human hearing range; see Audio S1 in the supporting information.

2. Methods

Infrasound instrumentation was located on the gondola of the NASA Ultra Long Duration Balloon, which was launched from Wanaka, New Zealand, on 16 May 2016. The balloon maintained a nominal altitude of 33 km,

10.1029/2018GL077737

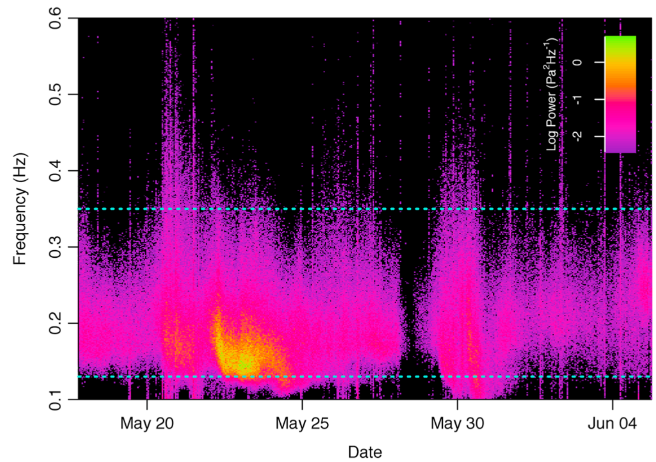

Figure 2. Fourier spectrogram of infrasound signals recorded during the 2016 Ultra Long Duration Balloon mission. The dashed blue lines represent the microbarom band. Spectrum window length was 1 hr. Powers were scaled to 0 °C and 1,000 mb to remove altitude-induced acoustic impedance effects.

with occasional downward excursions of several thousand meters. The infrasound recording system remained powered for 19.5 days, after which time the batteries were exhausted. The balloon remained in the air for a total of 46 days. The flight was terminated over Peru, and the data were recovered from the landing site.

The infrasound recording system consisted of an Omnirecs Datacube digitizer on the "high-resolution" setting recording at 200 samples per second at a gain of 64. Three InfraBSU infrasound microphones were used (Marcillo et al., 2012). One microphone had normal pressure polarity, one had reversed pressure polarity (accomplished by placing the mechanical low-pass filter on the opposite port), and one microphone was disabled by removing the mechanical filter entirely. The first two microphones were combined into a single channel via

$$M = \frac{M_{+} - M_{-}}{2} \tag{1}$$

where M_{+} is the microphone with normal polarity, M_{-} is the microphone with reversed polarity, and M is the virtual microphone that generated the data used in this paper. This method removes signals common between M_{+} and M_{-} such as vibration and electromagnetic interference. The microphones have not been calibrated to the pressure and temperature conditions during the flight, but the primary effect of the stratospheric environment should be to lower the corner period of the sensor. Since the ocean microbarom frequency range was already in the passband, the change in frequency response should have minimal impact on the instrument sensitivity.

The microphones and digitizer were each powered by separate Ultimate Lithium AA battery packs. Instruments were contained within high-density Styrofoam shipping boxes for thermal insulation. Internal temperature in the Datacube ranged from −26 to 7 ° C during the flight.

We used the European Center for Medium-Range Weather Forecasting (ECMWF) ERA5 analysis ocean wave product to identify times and locations where the ocean microbarom was being generated. The model indicated that the balloon crossed an ocean microbarom source during 23 May 2016 (Figure 3). The balloon-borne microphones recorded a 30 times increase in power in the ocean microbarom band during this time (see Figure 1). The pressure amplitudes of these waves were between 0.02 and 0.04 Pa (0.04 to 0.08 Pa peak to peak). This is equivalent to a pressure amplitude of about 0.2 to 0.4 Pa (0.4 to 0.8 Pa peak to peak) just above the ocean surface when acoustic impedance variation with altitude is accounted for. The Earth surface equivalent amplitude compares favorably with the 0.3-Pa average amplitude for the source as calculated by Rind (1977).

Acoustic energy flux at the balloon elevation can be estimated from the recorded pressure waveforms. Energy flux is a vector quantity, but direction of arrival cannot be determined from the single on board infrasound sensor package. To estimate the upgoing energy flux, we assume that the total acoustic energy flux E_t in the microbarom band consists of the sum of three terms:

10.1029/2018GL077737

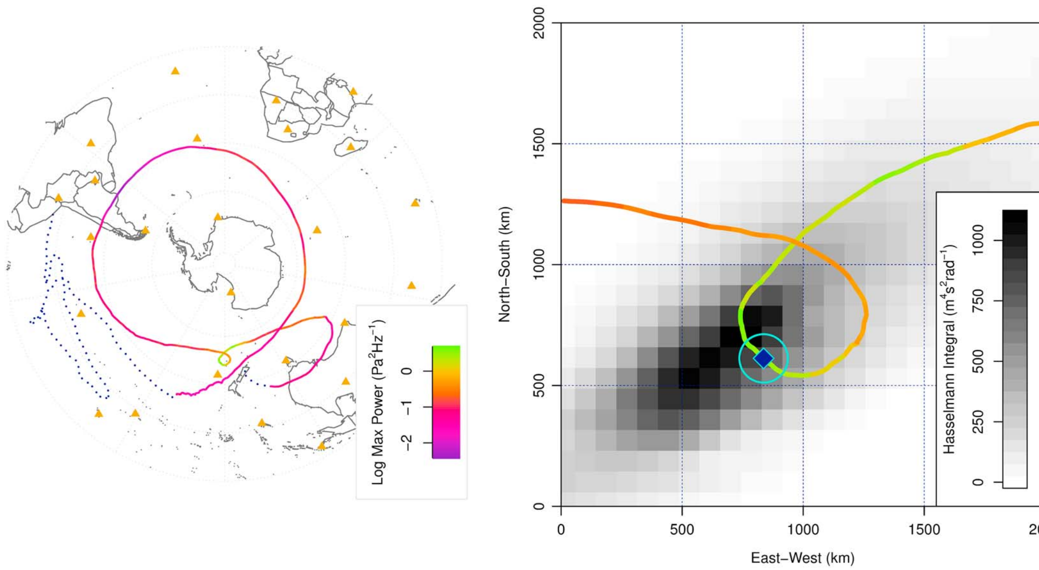

Figure 3. Flight path (left) and a snapshot of the microbarom source at 0600 UTC on 23 May 2016 (right). The balloon trajectory is color coded by the maximum power in the microbarom band over a 1-hr window. Dashed blue lines indicate the flight before and after the microbarom recording period, and yellow triangles are International Monitoring System infrasound stations. The inset (right) also shows the Hasselmann integral values summed over the microbarom band for 0600 UTC, 23 May 2016. The position of the balloon and the 100-km source averaging radius used in Figure 4 are also shown. Powers were scaled to 0 ° C and 1,000 mb to remove altitude-induced acoustic impedance effects.

$$\mathbf{E_t} = \mathbf{\hat{n}_d} E_d + \mathbf{\hat{n}_a} E_a + \mathbf{\hat{n}}_\epsilon E_\epsilon \tag{2}$$

where $\mathbf{\hat{n}}$ are unit vectors. We assume that energy E_d from the direct wave is arriving from below the balloon, so $\mathbf{\hat{n_d}}$ is directed straight upward. We assume a general level of ambient microbarom energy E_a coming from multiple distant sources

$$E_a \mathbf{\hat{n}_a} = \sum_{i=1}^{n} E_{a,i} \mathbf{\hat{n}_{a,i}} \tag{3}$$

none of which we know for certain. Finally, $E_\epsilon \mathbf{\hat{n}}_\epsilon$ is a fictitious vector quantity representing nonacoustic "noise" in the frequency band of interest.

The acoustic energy flux of a nondissipative acoustic plane wave is

$$\mathbf{E} = \frac{1}{2} \frac{\omega^2}{\rho c} p^2 \mathbf{\hat{n}} \tag{4}$$

where $\mathbf{E}$ is energy flux (W/m^2), ω is angular frequency, c is the local speed of sound, ρ is air density, and p is overpressure (Lighthill, 1978; Rayleigh, 1894). Energy flux in a given angular frequency band $\omega_a \ldots \omega_b$ can be estimated from the power spectrum via

$$\mathbf{E} = \frac{2}{N} \sum_{k=\omega_a}^{\omega_b} \frac{P(\omega_k)\omega_k^2}{\rho c} \tag{5}$$

where N is the number of data points in the signal. The power spectrum was estimated using the multitaper method (Lees & Park, 1995). The acoustic impedance term ρc was derived from the 0.25×0.25° Global Forecast System analysis model.

The acoustic power of the ocean microbarom source was estimated via the method of Smets and Evers (2014). First, we computed the Hasselmann integral of the directional ocean wave spectra in the microbarom band provided by the ERA5 model, then we averaged these values across a 100-km radius circle beneath the balloon. Acoustic power was calculated from the mean Hasselmann integral using equation (2) in Smets and Evers (2014), which takes into account the finite depth of the ocean (Waxler et al., 2007). Density and sound

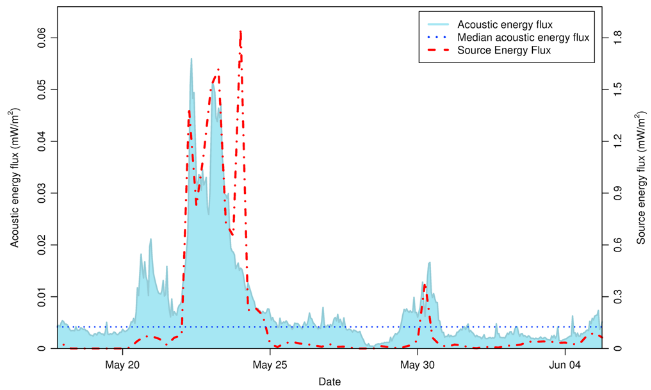

Figure 4. Energy flux in the microbarom band recorded on the balloon compared to the estimated microbarom source energy flux (Smets & Evers, 2014) averaged over a 100-km radius circle beneath the gondola. The dotted blue line is the median energy flux recorded throughout the whole flight.

speed were derived from temperature at 1,000 mb directly beneath the balloon provided by the Global Forecast System analysis model as well. Ocean bathymetry was derived from the ETOPO5 gridded elevation data (National Oceanic and Atmospheric Administration, 1988). For the solid earth density and shear wave velocity at the base of the ocean column, we used estimates following Kedar et al. (2008), with $\rho_b = 1.875$ g/cm^3 and $c_b = 2,100$ m/s, respectively.

3. Results and Conclusions

Figure 4 shows the total acoustic energy $\mathbf{E_t}$ in the ocean microbarom band compared to the mean microbarom source acoustic energy in a 100-km radius circle beneath the balloon. The ambient ocean microbarom energy $\mathbf{E_a}$ is estimated using the median of $\mathbf{E_t}$ during the recording period (the blue dotted line in the figure). This ambient energy from distant ocean microbarom sources contributes about 0.0042 mW/m^2 to the total energy flux calculation. The fictitious energy contribution from nonacoustic "noise" was calculated utilizing the mechanically disabled "control" microphone included in the balloon payload. This interference was in the range of 10^{-4} to 10^{-5} mW/m^2 and thus not visible on the scale of Figure 4.

Elevated ocean microbarom energy flux was observed between 20 and 25 May (the first 100 s in Audio S1). According to the ECMWF wave model, the balloon was above the ocean microbarom source region on 23 May. Subtracting the ambient term $\mathbf{E_a}$ yields a peak upgoing energy flux of 0.047 mW/m^2. The maximum acoustic energy flux occurred a day earlier with levels up to 0.052 mW/m^2, but according to the ECMWF wave model, the source region was not directly beneath the balloon. The wave model predicts a third pulse of energy that was not registered on the balloon sensors. The reason for this mismatch is not clear, but we speculate that it could be due to an inaccuracy in the ECMWF product or unfavorable infrasound propagation conditions at the edge of the 100-km region of investigation.

Results from our study suggest that the acoustic energy flux from the ocean microbarom event we observed is about a factor of 2 lower than estimates provided in Rind (1977). That study, which took place on ground microphones over 8 years, found that an average winter ocean microbarom episode in the North Atlantic generates an energy flux of 0.1 mW/m^2. Since Rind (1977) did not report the energy flux variance from episode to episode, it is unclear how the 0.05 mW/m^2 observed on the balloon compares with their observations. Regardless, the ocean microbarom episode observed on the balloon was probably less intense than the average event in the North Atlantic.

According to the ECMWF wave model, regions of elevated flux are hundreds to thousands of kilometers across and persist for several hours to several days. Previous studies indicate that acoustic energy from these areas is absorbed between 110 and 140 km (Rind, 1977), although nonlinear dissipation of the narrow band microbarom waveform could further concentrate the heating region (Krasnov et al., 2007). Our results suggest a 10^0- to 10^1-K thermospheric heating rate per day while the source persists. The temperature increase depends on both source strength and the region of the atmosphere in which acoustic dissipation occurs.

The energy flux calculations presented here rest upon several key assumptions. First, geometric attenuation is assumed to be minimal because of the large size of the source region (hundreds to thousands of kilometers) compared to the distance from the balloon-borne sensor to the lower thermosphere (80–110 km). This may bias the estimate high. Second, elevated energy levels during the source overflight are assumed to come solely from upgoing waves. However, it is possible that some of the energy was from waves trapped in the stratospheric duct from sources several hundred kilometers away from the balloon. Third, the sensors' amplitude and frequency response in the stratosphere is presumed to be the same as on the Earth's surface. After adjusting for acoustic impedance contrast effects, infrasound spectra for balloon-borne microphones appear similar to very low noise ground stations below about 2 Hz. Sensor frequency response is consistent with theoretical predictions in the limited test data available at stratospheric pressures (Bowman, 2016). Given these uncertainties, a conservative estimate of ocean microbarom energy flux during the source overflight is a value on the order of 10^{-2} mW/m^2. This is for one observation; quantification of the full range of ocean microbarom energy flux should be the target of future balloon-borne infrasound campaigns.

The impact of the energy flux of a given process depends both on the magnitude of the flux and the region where it is deposited. During the microbarom event, the upgoing acoustic energy flux of 0.05 mW/m^2 is about 3 orders of magnitude less than gravity wave energy flux from the troposphere during storms (Gossard, 1962). However, the maximum gravity wave dissipation rate in the mesosphere/lower thermosphere is estimated to be around 200 mW/kg (Fritts & Alexander, 2003), which is similar to the 330-mW/kg microbarom dissipation rate in Rind (1977). Atmospheric tides carry 1 to 10 times more energy than this microbarom event but dissipate at higher altitudes (Hines, 1965).

Following Rind (1977), we estimate that the heating rate in the lower thermosphere during the ocean microbarom event was ˜15 K/day. For comparison, nondissipative heating and cooling rates (e.g., solar absorption and infrared cooling) range from -10^1 to 10^1 K/day depending on latitude and time of year (Andrews et al., 1987; Medvedev & Fomichev, 1994). The inferred thermal effect from dissipating acoustic waves during the event described here is an order of magnitude larger than gravity wave heating in the mesosphere/lower thermosphere, since gravity wave dynamics produce competing heating and cooling effects (Becker & Schmitz, 2002).

The ocean microbarom is a global phenomenon, with multiple source regions active at any given time (Landès et al., 2012). Although the locations of these sources vary in space and time, we speculate that the cumulative effect of the ocean microbarom on the lower thermosphere could rival that of gravity waves and atmospheric tides. Persistent ocean microbarom source regions, such as south of Greenland during the Northern Hemisphere winter, may have a significant effect on the temperatures of the upper atmosphere directly above them. The ocean microbarom heating effect should be lowest over large landmasses.

Upper atmosphere thermal anomalies from the ocean microbarom should be observable using airglow methods. Airglow perturbations have been observed already for infrasound generated from wind-mountain interactions, volcanic activity, and severe storms (Pilger et al., 2013). We suggest that data from space-borne platforms such as the Sounding of the Atmosphere using Broadband Emission Radiometry instrument (Mlynczak, 1997) could be used to test our conclusions. Airglow measurements may provide a means of detecting ocean microbarom source regions when the acoustic velocity structure of the atmosphere precludes their localization via ground infrasound stations, for example, during the equinox (Landès et al., 2012).

The coupling of airglow measurements and ocean wave models in conjunction with targeted balloon-borne observation campaigns could provide a global specification of the ocean microbarom contribution to the thermal budget of the upper atmosphere. Current upper atmosphere models are climatologically based (Picone et al., 2002); they omit the contribution from such transient heating sources. However, future operational models of the thermosphere should incorporate the sea state; the extant ECMWF ocean wave specification makes this relatively straightforward.

The microbarom episode we recorded southeast of New Zealand produced an energy flux that was a factor of 2 less than the average energy flux from events in the North Atlantic described in Rind (1977). Our results support previous analyses suggesting that the ocean microbarom may heat the thermosphere on the order of 10^0 to 10^1 K/day, and this heating should be observable using airglow methods. Indeed, acoustic heating from the ocean microbarom represents a significant but poorly studied element of the upper atmosphere's thermal budget. Further balloon campaigns and ground-based studies will be required to determine the mean and variance of energy flux for microbarom episodes throughout the world, placing our initial results in context. Finally, the balloon-borne methods described here could be utilized to quantify the energy flux from orographically and meteorologically generated infrasound as well.

Acknowledgments
We thank the NASA Balloon Program Office and NASA Columbia Scientific Ballooning Facility for hosting our instrumentation on the 2016 Ultra Long Duration Balloon mission. Jordan Alpert at NOAA provided high-resolution Global Forecast System data for acoustic impedance calculations. Sharon Kedar assisted with interpretation. Jordan Bishop validated the mathematics and code implementation. Data from the ERA5 wave model were generated using the Copernicus Climate Change Service and are publicly available on the ECMWF web site. Our research was supported by Sandia National Laboratories, National Science Foundation (grants DGE-1144081, CDI-1125185, and AGS-1551999), and the University of North Carolina Department of Geological Sciences Martin Fund. Infrasound and balloon trajectory data are archived at datadryad.org under DOI 10.5061/dryad.40877s4. Sandia National Laboratories is a multimission laboratory managed and operated by National Technology and Engineering Solutions of Sandia, LLC., a wholly owned subsidiary of Honeywell International, Inc., for the U.S. Department of Energy's National Nuclear Security Administration under contract DE-NA0003525. The views expressed here do not necessarily reflect the views of the U.S. Government, the U.S. Department of Energy, or Sandia National Laboratories.

References

Andrews, D. G., Holton, J. R., & Leovy, C. B. (1987). *Middle atmosphere dynamics* . San Diego, CA: Academic Press.
Becker, E., & Schmitz, G. (2002). Energy deposition and turbulent dissipation owing to gravity waves in the mesosphere. *Journal of the Atmospheric Sciences*, *59*, 54–68.
Bowman, D. C. (2016). Infrasound from ground to space (Ph.D. thesis), The University of North Carolina at Chapel Hill.
Bowman, D. C., & Lees, J. M. (2017). A comparison of the ocean microbarom recorded on the ground and in the stratosphere. *Journal of Geophysical Research: Atmospheres*, *122*, 9773–9782. https://doi.org/10.1002/2017JD026474
Bowman, J. R., Baker, G. E., & Bahavar, M. (2005). Ambient infrasound noise. *Geophysical research letters*, *32*, L09803. https://doi.org/10.1029/2005GL022486
Campus, P., & Christie, D. R. (2010). Worldwide observations of infrasonic waves. In P. Campus & D. R. Christie (Eds.), *Infrasound monitoring for atmospheric studies* (pp. 185–234). Springer Science and Business Media.
Davies, K., & Jones, J. E. (1973). Acoustic waves in the ionospheric $F2$ region produced by severe thunderstorms. *Journal of Atmospheric and Terrestrial Physics*, *35*, 1787–1744. https://doi.org/10.1016/0021-9169(73)90052-4
Drobzheva, Y. V., & Krasnov, V. M. (2006). Acoustic energy transfer to the upper atmosphere from surface chemical and underground nuclear explosions. *Journal of Atmospheric and Solar-Terrestrial Physics*, *68*, 578–585. https://doi.org/10.1016/j.jastp.2005.03.023
Fritts, D. C., & Alexander, M. J. (2003). Gravity wave dynamics and effects in the middle atmosphere. *Reviews of Geophysics*, *41*(1), 1003. https://doi.org/10.1029/2001RG000106
Gossard, E. E. (1962). Vertical flux of energy into the lower ionosphere from internal gravity waves generated in the troposphere. *Journal of Geophysical Research*, *67*(2), 745–757. https://doi.org/10.1029/JZ067i002p00745
Hickey, M. P., Schubert, G., & Walterscheid, R. L. (2001). Acoustic wave heating of the thermosphere. *Journal of Geophysical Research*, *106*(A10), 21,543–21,548. https://doi.org/10.1029/2001JA000036
Hines, C. O. (1965). Dynamical heating of the upper atmosphere. *Journal of Geophysical Research*, *70*(1), 177–183. https://doi.org/10.1029/JZ070i001p00177
Kedar, S., Longuet-Higgens, M., Webb, F., Graham, N., Clayton, R., & Jones, C. (2008). The origin of deep ocean microseisms in the North Atlantic Ocean. *Proceedings of the Royal Society A*, *464*, 777–793. https://doi.org/10.1098/rspa.2007.0277
Krasnov, V. M., Drobzheva, Y. V., & Lastovicka, J. (2007). Acoustic energy transfer to the upper atmosphere from sinusoidal sources and a role of nonlinear processes. *Journal of Atmospheric and Solar-Terrestrial Physics*, *69*, 1357–1365. https://doi.org/10.1016/j.jastp.2007.04.011
Landès, M., Ceranna, L., Le Pichon, A., & Matoza, R. S. (2012). Localization of microbarom sources using the IMS infrasound network. *Journal of Geophysical Research*, *117*, D06102. https://doi.org/10.1029/2011JD016684
Lees, J. M., & Park, J. (1995). Multiple-taper spectral analysis: A stand-alone C-subroutine. *Computers & Geosciences*, *21*(2), 199–236.
Lighthill, J. (1978). *Waves in fluids*. Cambridge, UK: Cambridge University Press.
Lonzaga, J. B., Waxler, R. M., Assink, J. D., & Talmadge, C. L. (2015). Modelling waveforms of infrasound arrivals from impulsive sources using weakly non-linear ray theory. *Geophysical Journal International*, *200*, 1347–1361. https://doi.org/10.1093/gji/ggu479
Maeda, K. (1964). On the acoustic heating of the polar night mesosphere. *Journal of Geophysical Research*, *69*(7), 1381–1395. https://doi.org/10.1029/JZ069i007p01381
Marcillo, O., Johnson, J. B., & Hart, D. (2012). Implementation, characterization, and evaluation of an inexpensive low-power low-noise infrasound sensor based on a micromachined differential pressure transducer and a mechanical filter. *Journal of Atmospheric and Oceanic Technology*, *29*, 1275–1284. https://doi.org/10.1175/JTECH-D-11-00101.1
Medvedev, A. S., & Fomichev, V. I. (1994). Net radiative heating and diagnostics of the diabatic circulation in the 15–110 km height layer. *Journal of Atmospheric and Terrestrial Physics*, *56*(12), 1571–1584.
Mlynczak, M. G. (1997). Energetics of the mesosphere and lower thermosphere and the SABER experiment. *Advances in Space Research*, *20*(6), 1177–1183. https://doi.org/10.1016/S0273-1177(97)00769-2
National Oceanic and Atmospheric Administration (1988). Digital relief of the surface of the Earth (*Tech. rep.*): National Geophysical Data Center. Data Announcement 88-MGG-02.
Picone, J. M., Hedin, A. E., Drob, D. P., & Aikin, A. C. (2002). NRLMSISE-00 empirical model of the atmosphere: Statistical comparisons and scientific issues. *Journal of Geophysical Research*, *107*(A12), 1468. https://doi.org/10.1029/2002JA009430
Pilger, C., Schmidt, C., Streicher, F., Wüst, S., & Bittner, M. (2013). Airglow observations of orographic, volcanic, and meteorological infrasound signatures. *Journal of Atmospheric and Solar-Terrestrial Physics*, *104*, 55–66. https://doi.org/10.1016/j.jastp.2013.08.008
Rayleigh, J. W. S. B. (1894). *The theory of sound* (Vol. 2). London: Macmillan and Co.
Rind, D. (1977). Heating of the lower thermosphere by the dissipation of acoustic waves. *Journal of Atmospheric and Terrestrial Physics*, *39*, 445–456. https://doi.org/10.1016/0021-9169(77)90152-0
Rogers, P. H., & Gardner, J. H. (1980). Propagation of sonic booms in the thermosphere. *Journal of the Acoustical Society of America*, *67*(1), 78–91. https://doi.org/10.1121/1.383793
Semenov, A. I., Shefov, N. N., & Medvedeva, I. V. (2012). Orographic disturbances in the upper atmosphere. *Journal of Atmospheric and Solar-Terrestrial Physics*, *90-91*, 124–131. https://doi.org/10.1016/j.jastp.2012.05.009
Smets, P. S. M., & Evers, L. G. (2014). The life cycle of a sudden stratospheric warming from infrasonic ambient noise observations. *Journal of Geophysical Research: Atmospheres*, *119*, 12,084–12,099. https://doi.org/10.1002/2014JD021905
Walterscheid, R. L., Schubert, G., & Brinkman, D. G. (2003). Acoustic waves in the upper mesosphere and lower thermosphere generated by deep tropical convection. *Journal of Geophysical Research*, *108*(A11), 1392. https://doi.org/10.1029/2003JA010065
Waxler, R., & Gilbert, K. E. (2006). The radiation of atmospheric microbaroms by ocean waves. *The Journal of the Acoustical Society of America*, *119*(5), 2651–2664. https://doi.org/10.1121/1.2191607
Waxler, R., Gilbert, K. E., Talmadge, C., & Hetzer, C. (2007). The effects of the finite depth of the ocean on microbarom signals. In *8th International Conference on Theoretical and Computational Acoustics European Acoustics Association*, Crete, Greece.